

## Journal Name

Crossmark

PAPER

RECEIVED

dd Month yyyy

REVISED

dd Month yyyy

## Development of Low-Noise Two-stage dc-SQUID for TES Detector Readout

Nan Li<sup>1</sup> , Mengjie Song<sup>1</sup> , Sixiao Hu<sup>1</sup> , Wentao Wu<sup>2</sup> , Songqing Liu<sup>3,4</sup> , Tangchong Kuang<sup>5</sup> , Yudong Gu<sup>1</sup> , Xiangxiang Ren<sup>5</sup> , Xufang Li<sup>1</sup> , He Gao<sup>1,\*</sup> , Zhengwei Li<sup>1,\*</sup> , and Congzhan Liu<sup>1,\*</sup> 

<sup>1</sup>State Key Laboratory of Particle Astrophysics, Institute of High Energy Physics, CAS, 19B Yuquan Road, Shijingshan District, 100049, Beijing, China

<sup>2</sup>State Key Laboratory of Materials for Integrated Circuits, Shanghai Institute of Microsystem and Information Technology, Chinese Academy of Sciences, Shanghai 200050, China

<sup>3</sup>Shandong University, Jinan, Shandong 250100, China

<sup>4</sup>Shandong Institute of Advanced Technology (SDIAT), Jinan, Shandong 250100, China

<sup>5</sup>Key Laboratory of Particle Physics and Particle Irradiation (MOE), Institute of Frontier and Interdisciplinary Science, Shandong University, Qingdao, Shandong, 266237, China

\* Author to whom any correspondence should be addressed.

**E-mail:** hgao@ihep.ac.cn, lizw@ihep.ac.cn and liucz@ihep.ac.cn

**Keywords:** Two-stage dc-SQUID, cryogenic readout electronics, transition edge sensors

**Abstract**

Direct-current superconducting quantum interference devices (dc-SQUIDs) are one of the most sensitive magnetic detectors. These sensors are extensively used in the readout of superconducting transition edge sensors (TESs), which are used for the detection of weak signals. A cosmic microwave background (CMB) polarization telescope operating in 22-48 GHz is currently under developing. The TESs calorimeter of the telescope will be readout by a time-division multiplexer (TDM) SQUID readout system. We develop a two-stage dc-SQUID amplifier circuit, comprising an input-stage SQUID with 4 SQUID cells and a series SQUID array (SSA) with 100 SQUID cells. This configuration has been shown to achieve extremely high signal gain while effectively controlling system noise. We assess the system noise at 300 mK in an adiabatic demagnetisation refrigerator (ADR). The measured magnetic flux noise of the two-stage SQUID circuit system is approximately  $0.3 \mu\Phi_0/\sqrt{Hz}$  at 10 kHz. The current noise equivalent to the input coil of input SQUID is about  $2.4 pA/\sqrt{Hz}$ . This result meets the low-noise readout requirements of the CMB TES and other applications with TES detectors.

**1 Introduction**

Transition-edge sensors (TESs) have been applied in numerous fields due to extremely low thermal noise[1, 2, 3, 4]. TESs are widely used in weak signal detection experiments, such as millimeter wave[5], X-ray[6, 7],  $\gamma$ -ray[8], cold dark matter[9], neutrinoless double beta decay[10], and so on. The Ali primordial gravitational wave detection project is developing TES detection technology to search primordial gravitational waves[11]. Due to the influence of Galactic foreground, B-mode polarization from primordial gravitational waves has not yet been accurately observed [12]. The Ali primordial gravitational wave detection project is designing a telescope to detect CMB polarization in the frequency range of 22 to 48 GHz (AliCPT-40G) to study Galactic foreground. The AliCPT-40G telescope will deploy approximately 600 TES detectors on the focal plane, utilizing a time-division multiplexing (TDM) electronic system based on two-stage direct-current superconducting quantum interference devices (dc-SQUIDs). Dc-SQUID has ultra sensitive responses to weak magnetic signals and notably low noise performance, which is suitable for TES readout[13, 14, 15]. The working state of TES is near superconducting[16], which enables sensitive response to weak signals. TES exhibits extremely low thermal noise, typically ranging from tens to hundreds of  $pA/\sqrt{Hz}$  with excess noise[17, 18, 19, 20]. Thus in order to ensure the high performance of TES, it is necessary to control the total noise of the two-stage dc-SQUID readout system below  $10 pA/\sqrt{Hz}$ , thereby preventing it from becoming the major system noise source.

We have developed a two-stage dc-SQUID circuit capable of reading out CMB TES calorimeters and compatible with other most TES applications. The paper is organized as follows: Section 2 describes the chips design of the input SQUID and SSA. Section 3 presents the measurements of design parameters and system performance. Section 4 provides the conclusions of the paper.

## 2 Input SQUID and SSA design

A two-stage dc-SQUID, comprising an input SQUID formed by one or several SQUID cells in series and a series SQUID array (SSA) with numerous cascaded SQUID cells, combined with an integrating amplifier circuit, forms a flux-locked loop circuit [21, 22, 23] can achieve extremely high signal gain while effectively controlling system noise, as shown in Figure 1. The blue area in

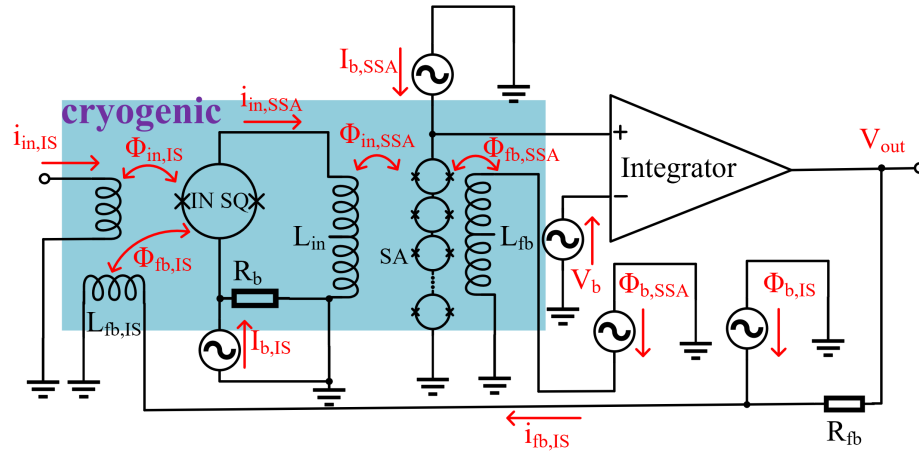


**Figure 1.** Two-stage dc-SQUID circuit for TES readout. The current signal  $i_{in,IS}$  flowing through the TES is converted into a magnetic flux signal  $\Phi_{in,IS}$  by the input coil  $L_{in,IS}$  of the input SQUID. This flux signal cancels the feedback magnetic flux signal  $\Phi_{fb,IS}$ . Flux-locked loop linearly amplifies the TES signal based on the room-temperature integrating amplifier.

Figure 1 indicates the low-temperature region, while the red arrow denotes the primary signal transmission paths and the locking point tuning signals. The input SQUID loop exhibits a high current sensitivity relative to the input coil, which allows for more effective amplification of the weak current signals flowing through the TES[24]. The primary noise sources in the readout system are input SQUID and SSA noise and room-temperature amplifier noise. The large flux conversion coefficient  $I_\Phi$  effectively reduces noise contributions from the SSA to the TES. After further amplification by the SSA, the signal amplitude can reach hundreds of  $\mu V$  or even several  $mV$ , ultimately amplified again by the room-temperature amplifier for final readout. SSA with numerous SQUID cells, can exhibit a very large flux conversion coefficient  $V_\Phi$ , which effectively reduces the noise contribution of the room-temperature amplifier to the system[25].

The input SQUID is designed as double-transformer type [26, 27, 28], as shown in Figure 2 (a),(b), it consists of 4 real SQUID cells, flanked by 2 dummy SQUID cells at either end. Each cell is a first-order series gradiometer formed by two nearly rectangular washers. The hole dimension of each washer is  $40 \mu m \times 12 \mu m$ . The input coil, running on top of both washers, is coupled to an input transformer so that the relatively low SQUID inductance ( $140 pH$ ) can be matched with a relatively high input inductance. The feedback coil is located at both sides of the washers. On-chip low-pass filters are added to the coils. The Josephson junction size of input SQUID is  $2.5 \mu m \times 2.5 \mu m$ , cooling fins [29] are connected to the shunt resistors of junctions to enlarge the cooling area for minimizing the hot electron effect below  $1 K$ . The asymmetric bias injection technique [30] were used in each SQUID cell, and a lot of dummy structures were added to enhance the gradiometry of SQUID: The SSA consists of a 100 SQUID cells (4 rows  $\times$  25 real SQUID cells), as shown in Figure 2 (c),(d). Each cell is designed as a first-order series gradiometer as well. It is highly similar to the input SQUID cell, except for the junction size of  $3 \mu m \times 3 \mu m$  and each washer hole dimensions of  $40 \mu m \times 9 \mu m$ , and there are also low-pass filters near the output pads. The detailed design parameters of input SQUID and SSA are summarized in Table 1 and 2. The proposed input SQUID and SSA devices were fabricated with high-quality Nb/AlAlOx/Nb trilayer JJs in a standard fabrication process at the Superconducting Electronics Facility (SELF), of the Shanghai Institute of Microsystem and Information Technology (SIMIT). The Nb/Al-AlOx/Nb trilayer is deposited in situ using magnetron sputtering with a critical current density  $J_c$  of about 1.3

$\mu A/\mu m^2$  (at 300 mK) and a specific capacity Cs of  $40.5 fF/\mu m^2$ . The detailed process steps have been reported in previous works [25, 31].

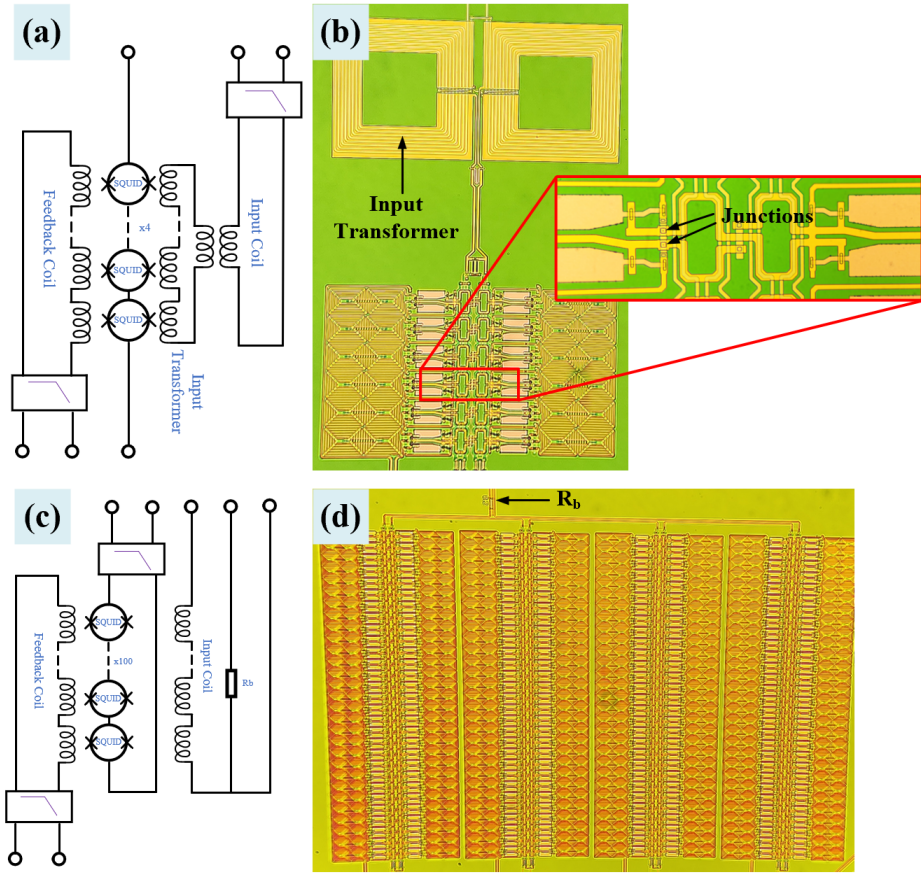


**Figure 2.** Schematic of the dc-SQUID chips. (a) Input SQUID schematic; (b) Input SQUID board layout; (c) SSA schematic; (d) SSA board layout.

**Table 1.** Design parameters of the input SQUID at 300 mK.

Parameters	Designed value
Critical current of input SQUID $2I_{c0,IS}$	$16 \mu A$
SQUID loop inductance $L_{s,IS}$	$140 pH$
$\beta_c$ of Junctions	0.23
$\beta_L$ of the input SQUID cell	1.10
Input coil inductance $L_{in,IS}$	$39.6 nH$
Current sensitivity of Input SQUID $1/M_{in,IS}$	$8.1 \mu A/\Phi_0$
Feedback coil coupling $1/M_{fb,IS}$	$39.7 \mu A/\Phi_0$

### 3 Measurement and discussion

System noise is the most significant factor affecting the performance of TES. The system noise contributions in a two-stage dc-SQUID primarily include intrinsic flux noise from the input SQUID and SSA, as well as noise from room-temperature readout electronics. Based on the circuit signal transmission model of the two-stage dc-SQUID (Figure 1), the system noise  $NEI_{sys}$  can be characterized by the equivalent current noise density of the input coil connected to the input SQUID, as shown in Equation 1.

$$NEI_{sys} = \sqrt{NEI_{IS}^2 + NEI_{SSA}^2 + NEI_{elec}^2} \quad (1)$$

The current sensitivity between the the input coil of input SQUID and its junction loop determines the gain for converting the current signal flowing through the TES into the magnetic flux signal. Therefore, it is a crucial parameter affecting the transmission of system noise. The transfer function relating the intrinsic flux noise density  $n_{IS}$  of the input SQUID to the equivalent current

**Table 2.** Design parameters of SSA at 300 mK.

Parameters	Designed value
Critical current of SSA $2I_{c0,SSA}$	23 $\mu A$
SQUID loop inductance $L_{s,SSA}$	120 $pH$
$\beta_c$ of Junctions	0.26
$\beta_L$ of the SSA cell	1.36
Current sensitivity of SSA $1/M_{in,SSA}$	27.4 $\mu A/\Phi_0$
Feedback coil coupling $1/M_{fb,IS}$	37.6 $\mu A/\Phi_0$

noise density  $NEI_{IS}$  referring to its input coil is given by Equation 2.

$$NEI_{IS} = \frac{n_{IS}}{M_{in,IS}}. \quad (2)$$

Additionally, the flux conversion coefficients  $I_\Phi$  of input SQUID and  $V_\Phi$  of SSA are equally important parameters affecting the system noise. The contribution of SSA to the system noise  $NEI_{SSA}$  can be converted based on its intrinsic flux noise  $n_{SSA}$ , as shown in Equation 3.

$$NEI_{SSA} = \frac{n_{SSA}}{M_{in,SSA} I_\Phi M_{in,IS}}. \quad (3)$$

The  $NEI_{SSA}$  is inversely correlated with the flux conversion coefficient  $I_\Phi$  which is strongly dependent on the working point [25]. It is evident that an increase in the flux conversion coefficient results in a reduction in the contribution of back-end noise. Room-temperature electronic noise undergoes further attenuation via the SSA's magnetic flux conversion coefficient  $V_\Phi$ , resulting in a lower system contribution  $NEI_{elec}$ , as shown in Equation 4.

$$NEI_{elec} = \frac{n_{elec}}{V_\Phi M_{in,SSA} I_\Phi M_{in,IS}}. \quad (4)$$

Room-temperature electronic noise  $n_{elec}$  primarily originates from the voltage noise and current noise of the preamplifier.

The current sensitivities,  $V_\Phi$  and  $I_\Phi$  can be obtained by measuring the magnetic flux response  $V$ - $\Phi$  curves of the SQUIDs. The  $V$ - $\Phi$  characteristics of the fabricated input SQUID and SSA chips were measured at 300 mK within ADR system. The input SQUID and SSA were each glued to a printed circuit board (PCB) and mounted on the 300 mK gold-plated copper cold plate in ADR. Each pad on the chips was connected to the PCB by aluminum bonding wires, as illustrated in Figure 3. The chips were finally equipped with a superconducting Nb can as a shield from stray magnetic fields.

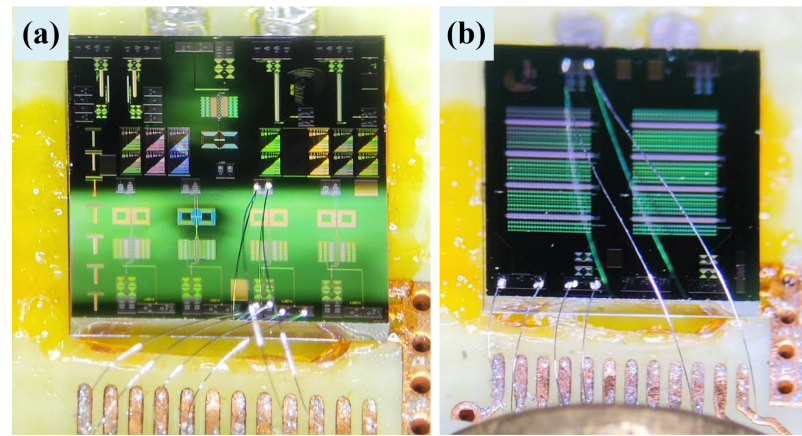


**Figure 3.** Input SQUID (a) and SSA (b) are connected to pads of PCB via wire-bonding. They are installed on the 300 mK copper plate in ADR.

Magnicon electronics provide all bias currents and coil reference flux inputs to input SQUID and SSA, respectively. The  $V$ - $\Phi$  response of the input SQUID and SSA measured under different bias currents is shown in Figure 4. It can be seen that the current sensitivity between the junction loop and the input coil, as well as the feedback coil, of input SQUID are  $8 \mu A/\Phi_0$  and  $40 \mu A/\Phi_0$  respectively. The current sensitivity between the SSA's loop and the input coil and feedback coil

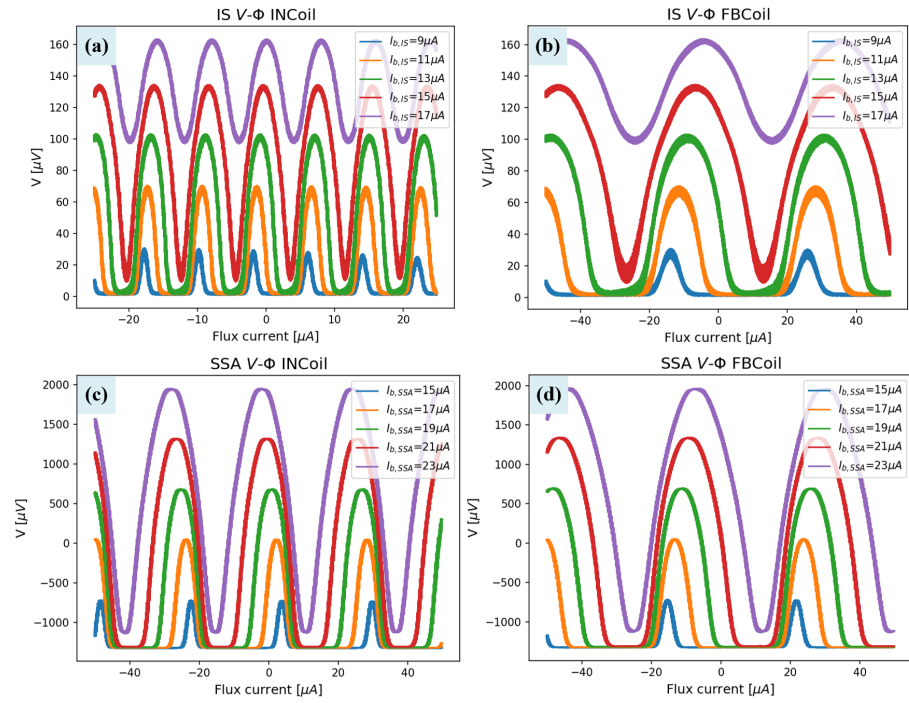


**Figure 4.** The  $V\Phi$  characteristics of the input SQUID and SSA were measured at  $300\text{ mK}$  in ADR. The results correspond to the input coil (a) and feedback coil (b) of the input SQUID, and the input coil (c) and feedback coil (d) of the SSA.

are  $27\text{ }\mu\text{A}/\Phi_0$  and  $38\text{ }\mu\text{A}/\Phi_0$  respectively. The input SQUID and SSA exhibit maximum voltage swings and maximum flux conversion coefficients near  $15\text{ }\mu\text{A}$  and  $23\text{ }\mu\text{A}$  current bias points respectively, which is proximate to the expected critical currents ( $2I_{c0,IS}$  and  $2I_{c0,SSA}$ ).

In order to achieve enhanced system noise performance, the two-stage dc-SQUID was bonded (as shown in Figure 4) and also placed at a temperature of  $300\text{ mK}$  in ADR. The measured results were based on ultra low-noise Magnicon flux-locked loop readout circuit, which are of  $0.33\text{ nV}/\sqrt{\text{Hz}}$  voltage noise and  $2.6\text{ pA}/\sqrt{\text{Hz}}$  current noise[32]. The SSA exhibits a maximum voltage



**Figure 5.** The input SQUID is connected to the SSA via wire-bonding. They are installed on the Nb-shielded PCB of Magnicon at the  $300\text{ mK}$  copper plate in ADR.

swing at  $300\text{ mK}$ , which is approximately  $3\text{ mV}$  at a current bias of  $23\text{ }\mu\text{A}$ . At the optimal working point, the flux conversion coefficient  $V_\phi$  has the maximum value, which is approximately  $10\text{ mV}/\Phi_0$ , as shown in Figure 6 (a). In a two-stage dc-SQUID circuit, the dynamic resistance of the input SQUID is substantially greater than the parallel resistor  $R_b$ , which is  $0.2\text{ }\Omega$  in our design. According to Thevenin's theorem, the bias current will be equivalent to a voltage bias (as shown in

Figure 1). Under a  $4 \mu V$  voltage bias, the maximum current swing measured through the input SQUID is approximately  $7 \mu A$ , which is primarily constrained by the magnitude of the approximately linear gain interval  $\Delta I_{in,SSA}$  around the SSA working point. The maximum value of  $I_\Phi$ , at the working (locking) point, is approximately  $45 \mu A/\Phi_0$ , as shown in Figure 6 (b). The

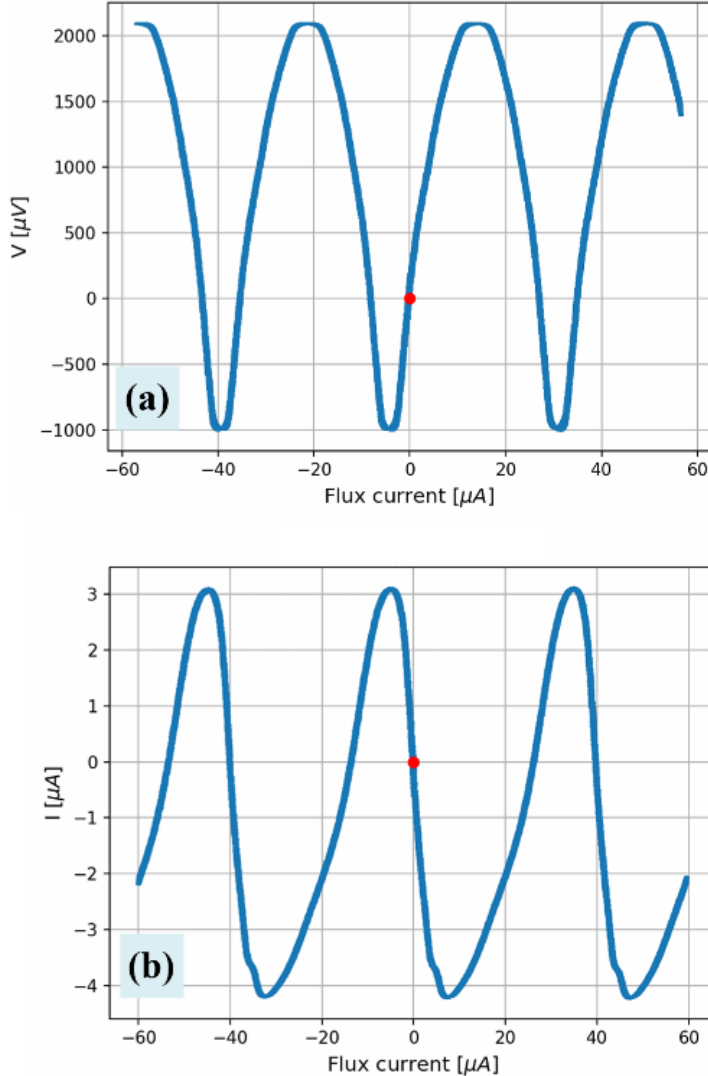


**Figure 6.** Tuning of the working points for the SSA (a) and input SQUID (b) with feedback coils. The maximum voltage swing of the SSA is approximately  $3 mV$  and the maximum  $V_\Phi$  is about  $10 mV/\Phi_0$ . The maximum current swing of the input SQUID is approximately  $7 \mu A$  and the maximum  $I_\Phi$  is about  $45 \mu A/\Phi_0$  at  $300 mK$ . The red dots indicate the working points.

input SQUID  $V$ - $\Phi$  curve has minor distortion at its base. One possible explanation is that the  $\beta_c$  exceeds the designed value, thereby inducing Josephson high-frequency oscillation with microstrip resonators[33].

Figure 7 shows the noise of two-stage dc-SQUID circuit with  $10 k\Omega$  and  $100 k\Omega$  feedback resistors separately. The flat noise power density is about  $1 \mu\Phi_0/\sqrt{Hz}$  at  $1 kHz$  with  $10 k\Omega$  feedback resistor. It is about  $0.5 \mu\Phi_0/\sqrt{Hz}$ , when the feedback resistor is  $100 k\Omega$ . This is reasonable. According to the linear transfer function of flux-locked loop ( $i_{in} = u_{out}/R_{fb}$ ), the larger the feedback resistance  $R_{fb}$ , the smaller the influence of noise equivalent current referring to the input coil of input SQUID  $i_{in}$  from the voltage of the feedback (or readout) circuit  $u_{out}$ . The flat noise power density is about  $0.3 \mu\Phi_0/\sqrt{Hz}$  at  $10 kHz$  after flux-locked and with  $100 k\Omega$  feedback resistor. The system noise equivalent current  $NEI_{sys}$ , which can be calculated by Equation 2, is about  $4 pA/\sqrt{Hz}$  at  $1 kHz$  and  $2.4 pA/\sqrt{Hz}$  at  $10 kHz$ , which is significantly lower than the typical noise level of  $100 pA/\sqrt{Hz}$  for a TES system. Figure 4 shows the dynamic resistance value of the SSA  $R_{dyn,SSA}(\Phi) = V_{SSA}(\Phi)/I_{b,SSA}$  at locking point, which is about  $50 \Omega$ .  $V_{SSA}(\Phi)$  is the voltage swing at different flux input.  $I_{b,SSA}$  is the bias current of SSA. Thus the

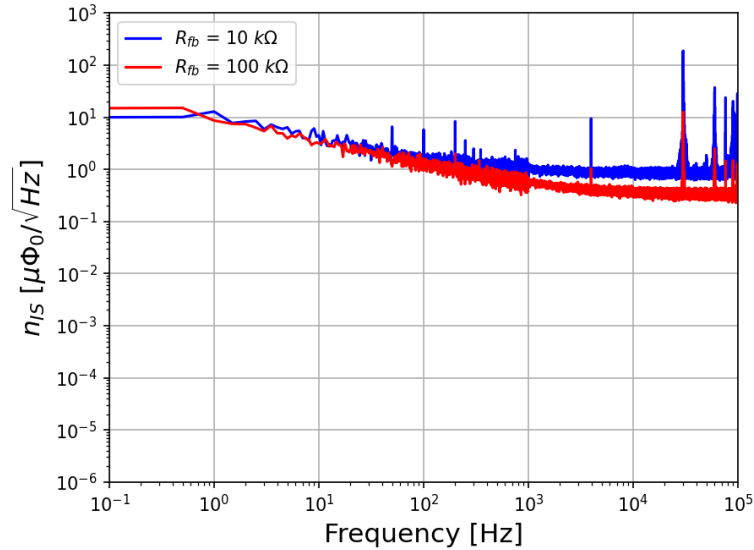


**Figure 7.** The flux-locked noise of the two-stage dc-SQUID circuit with different feedback resistors at 300 mK.

total voltage noise of Magnicon electronics  $n_{elec}$  is about  $0.35 \text{ nV}/\sqrt{\text{Hz}}$ , which can be calculated by Equation 5. And the noise referring to the input coil of input SQUID  $NEI_{elec}$  is about  $0.17 \text{ pA}/\sqrt{\text{Hz}}$ , which is negligible.

$$n_{elec} = \sqrt{n_v^2 + (n_i R_{dyn,SSA})^2}. \quad (5)$$

We also measured the flux-locked noise of SSA without input SQUID at the same temperature in ADR. The intrinsic noise of SSA system is about  $0.25 \mu\Phi_0/\sqrt{\text{Hz}}$  at 10 kHz, as shown in Figure 8. The  $NEI_{SSA}$  is about  $1.2 \text{ pA}/\sqrt{\text{Hz}}$  referring to input coil of input SQUID based on Equation 3. The input SQUID noise equivalent current contribution  $NEI_{IS}$  can be calculated to be

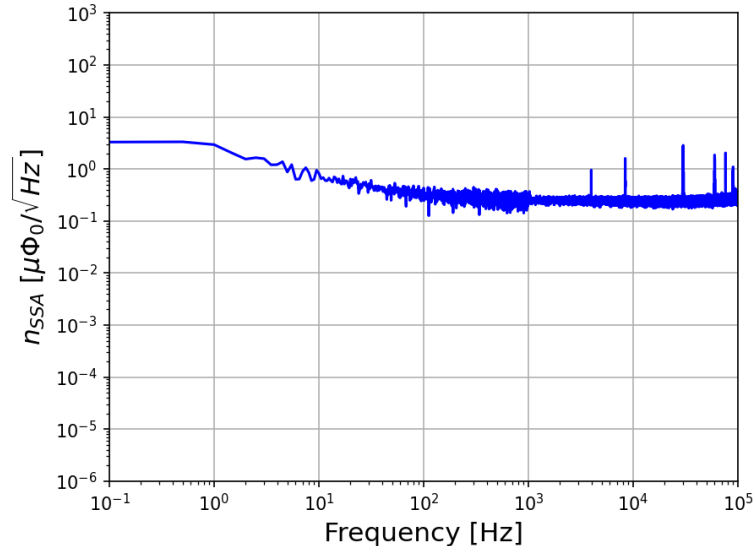


**Figure 8.** SSA system noise at 300 mK with 100 kΩ feedback resistor in ADR.

approximately  $2.1 \text{ pA}/\sqrt{\text{Hz}}$  at 10 kHz referring to its input coil. Therefore, in our two-stage dc-SQUID readout system, the noise contributions from room temperature electronics and even SSA, are negligible.

#### 4 Conclusion

We have developed a two-stage dc-SQUID amplifier with exceptionally low noise. The system noise equivalent current density is as low as  $2.4 \text{ pA}/\sqrt{\text{Hz}}$ . The input SQUID exhibits not only a high current sensitive of  $8 \mu\text{A}/\Phi_0$ , but also a substantial flux conversion coefficient  $I_\Phi \approx 45 \mu\text{A}/\Phi_0$ , which ensures the noise contribution of SSA is merely  $1.2 \text{ pA}/\sqrt{\text{Hz}}$  referring to the input coil of input SQUID. The noise contribution of input SQUID is about  $2.1 \text{ pA}/\sqrt{\text{Hz}}$  referring to its input coil. The SSA employs a structure with 100 dc-SQUID cells connected in series, achieving a flux conversion coefficient  $V_\Phi$  of  $10 \text{ mV}/\Phi_0$ . The room-temperature electronics noise contribution is about  $0.17 \text{ pA}/\sqrt{\text{Hz}}$ , which is negligible. The two-stage dc-SQUID circuit can satisfy the requirements of TDM readout system, which will be used in AliCPT-40G in the near future. Also, it can be applied in detection of X/ $\gamma$ -rays.

#### Funding

This work is supported by the National Key Research and Development Program of China (Grant No.2021YFC2203400), the National Natural Science Foundation of China (Grant No 12173040), Youth Innovation Promotion Association CAS 2021011, Scientific Instrument Developing Project of the Chinese Academy of Sciences (Grant No.YJKYYQ20190065, No.PTYQ2025TD0021), and the National Key Research and Development Program of China (Grant No.2022YFC2204902, No.2022YFC2204900).

#### References

- [1] Yan Li, WenDa Huang, Shuanghui Shi, Jiahui Gu, Jingyi Liu, Xiaohan Yu, and Jiping Zeng. The level structure of  $^{76}\text{Se}$  from  $^{76}\text{Br}$   $\gamma$ -decay. *Nuclear Science and Techniques*, 9(4):199–208, 1998. Web: <http://www.nst.sinap.ac.cn/article/id/5568>.
- [2] Weifan Yang, Zhizheng Zhao, Zongwei Li, and Wantong Mou. New gamma rays from decay of  $^{189}\text{W}$ . *Nuclear Science and Techniques*, 6(4):222–224, 1995. Web: <https://api.semanticscholar.org/CorpusID:94061252>.
- [3] Davide Vaccaro et al. System performance of a cryogenic test-bed for the time-division multiplexing readout for the newathena x-ray integral field unit. *Journal of Astronomical Telescopes, Instruments, and Systems*, 10(4):046002–046002, 2024. DOI: [10.48550/arXiv.2409.05643](https://doi.org/10.48550/arXiv.2409.05643).
- [4] Jiejia Liu et al. Preliminary design of detector assembly for dixe. *Journal of Low Temperature Physics*, 216(1):273–284, Jul 2024. DOI: [10.1007/s10909-024-03131-z](https://doi.org/10.1007/s10909-024-03131-z).
- [5] Yongping Li, Yang Liu, Si-Yu Li, Hong Li, and Xinmin Zhang. Tibet's ali: a new window to detect the cmb polarization. *arXiv preprint arXiv:1709.09053*, 2017. DOI: [10.48550/arXiv.1709.09053](https://doi.org/10.48550/arXiv.1709.09053).
- [6] Luciano Gottardi and Kenichiro Nagayashi. A review of x-ray microcalorimeters based on superconducting transition edge sensors for astrophysics and particle physics. *Applied Sciences*, 11(9):3793, 2021. DOI: [10.3390/app11093793](https://doi.org/10.3390/app11093793).
- [7] Zhang Shuo, Cui Wei, Jin Hai, Chen Liu-Biao, Wang Jun-Jie, Wu Wen-Tao, Wu Bing-Jun, Xia Jing-Kai, Song Yan-Ru, Yang Jin-Ping, et al. Development of basic theory and application of cryogenic x-ray spectrometer in light sources and x-ray satellite. *Acta Physica Sinica*, 70(18), 2021. DOI: [10.7498/aps.70.20210350](https://doi.org/10.7498/aps.70.20210350).
- [8] Shuo Zhang, Jing-Kai Xia, Tao Sun, Wen-Tao Wu, Bing-Jun Wu, Yong-Liang Wang, Robin Cantor, Ke Han, Xiao-Peng Zhou, Hao-Ran Liu, et al. Transition edge sensor-based detector: from x-ray to  $\gamma$ -ray. *Nuclear Science and Techniques*, 33(7):84, 2022. DOI: [10.1007/s10909-024-03131-z](https://doi.org/10.1007/s10909-024-03131-z).
- [9] Junsong Cang, Yu Gao, and Yin-Zhe Ma. Probing dark matter with future cmb measurements. *Physical Review D*, 102(10):103005, 2020. DOI: [10.1103/PhysRevD.102.103005](https://doi.org/10.1103/PhysRevD.102.103005).
- [10] G Bratrud, CL Chang, R Chen, E Cudmore, E Figueiroa-Feliciano, Z Hong, KT Kennard, S Lewis, M Lisovenko, LO Mateo, et al. First demonstration of a tes based cryogenic  $^{32}\text{Mg}$  detector for neutrinoless double beta decay search. *arXiv preprint arXiv:2406.02025*, 2024. DOI: [10.1140/epjc/s10052-025-13844-4](https://doi.org/10.1140/epjc/s10052-025-13844-4).

- [11] Janet L Weiland, Graeme E Addison, Charles L Bennett, Mark Halpern, and Gary Hinshaw. Polarized synchrotron foreground assessment for cmb experiments. *The Astrophysical Journal*, 936(1):24, 2022. DOI: [10.3847/1538-4357/ac83ab](https://doi.org/10.3847/1538-4357/ac83ab).
- [12] R Adam, Peter AR Ade, N Aghanim, MIR Alves, M Arnaud, M Ashdown, J Aumont, C Baccigalupi, AJ Banday, RB Barreiro, et al. Planck 2015 results-x. diffuse component separation: Foreground maps. *Astronomy & Astrophysics*, 594:A10, 2016. DOI: [10.1051/0004-6361/201525967](https://doi.org/10.1051/0004-6361/201525967).
- [13] Kent D Irwin. Squids and transition-edge sensors. *Journal of Superconductivity and Novel Magnetism*, 34(6):1601–1606, 2021. DOI: [10.1007/s10948-020-05730-9](https://doi.org/10.1007/s10948-020-05730-9).
- [14] ZF Feng, XF Zhou, QX Ma, W Zhang, PZ Li, Z Wang, JQ Zhong, W Miao, Y Ren, QJ Yao, et al. Development of second-order gradient dc squids for the readout of superconducting tes detectors. In *Infrared, Millimeter-Wave, and Terahertz Technologies XII*, volume 13726, pages 37–43. SPIE, 2025. DOI: [10.1117/12.3073803](https://doi.org/10.1117/12.3073803).
- [15] Mikko Kiviranta and Leif Grönberg. Components for multiplexed dc-squid readouts of transition edge sensor arrays. *IEEE Transactions on Applied Superconductivity*, 33(5):1–6, 2023. DOI: [10.1109/TASC.2023.3265909](https://doi.org/10.1109/TASC.2023.3265909).
- [16] Kent D Irwin and Gene C Hilton. Transition-edge sensors. In *Cryogenic particle detection*, pages 63–150. Springer, 2005. DOI: [10.1007/10933596\\_3](https://doi.org/10.1007/10933596_3).
- [17] Joel N Ullom, William B Doriese, Gene C Hilton, James A Beall, Steven Deiker, Kent D Irwin, Carl D Reintsema, Leila R Vale, and Yizi Xu. Suppression of excess noise in transition-edge sensors using magnetic field and geometry. *Nuclear Instruments and Methods in Physics Research Section A: Accelerators, Spectrometers, Detectors and Associated Equipment*, 520(1-3):333–335, 2004. DOI: [10.1016/j.nima.2003.11.260](https://doi.org/10.1016/j.nima.2003.11.260).
- [18] A Luukanen, KM Kinnunen, AK Nuottajärvi, HFC Hoevers, WM Bergmann Tiest, and Jukka P Pekola. Fluctuation-limited noise in a superconducting transition-edge sensor. *Physical review letters*, 90(23):238306, 2003. DOI: [10.1103/PhysRevLett.90.238306](https://doi.org/10.1103/PhysRevLett.90.238306).
- [19] Joel N Ullom, William B Doriese, Gene C Hilton, James A Beall, Steven Deiker, WD Duncan, L Ferreira, Kent D Irwin, Carl D Reintsema, and Leila R Vale. Characterization and reduction of unexplained noise in superconducting transition-edge sensors. *Applied Physics Letters*, 84(21):4206–4208, 2004. DOI: [10.1063/1.1753058](https://doi.org/10.1063/1.1753058).
- [20] Abigail Wessels, Kelsey Morgan, Johnathon D Gard, Gene C Hilton, John AB Mates, Carl D Reintsema, Daniel R Schmidt, Daniel S Swetz, Joel N Ullom, Leila R Vale, et al. A model for excess johnson noise in superconducting transition-edge sensors. *Applied physics letters*, 118(20), 2021. DOI: [10.1063/5.0043369](https://doi.org/10.1063/5.0043369).
- [21] Richard P Welty and John M Martinis. Two-stage integrated squid amplifier with series array output. *IEEE Transactions on Applied Superconductivity*, 3(1):2605–2608, 2002. DOI: [10.1109/77.233523](https://doi.org/10.1109/77.233523).
- [22] Robin Cantor, Luke P Lee, Andrey Matlashov, and Vladimir Vinetskiy. A low-noise, two-stage dc squid amplifier with high bandwidth and dynamic range. *IEEE transactions on applied superconductivity*, 7(2):3033–3036, 1997. DOI: [10.1109/77.621971](https://doi.org/10.1109/77.621971).
- [23] Yifei Zhang, Zhengwei Li, Mengxian Zhang, Guofu Liao, Zhouhui Liu, Yu Xu, Nan Li, Liangpeng Xie, Junjie Zhou, Xufang Li, et al. Fabrication and characterization of x-ray tes detectors based on annular almn alloy films. *Journal of Low Temperature Physics*, pages 1–13, 2025. DOI: [10.1007/s10909-012-0574-y](https://doi.org/10.1007/s10909-012-0574-y).
- [24] Schmelz Matthias, Shvab Vitaliy, Peiselt Katja, Kunert Jürgen, Zakosarenko Vyacheslav, Stöhlker Thomas, Oelsner Gregor, and Stoltz Ronny. Highly sensitive dc squid arrays for the readout of optical tes at mk temperatures. *IEEE Transactions on Applied Superconductivity*, 2025. DOI: [10.1109/TASC.2025.3543941](https://doi.org/10.1109/TASC.2025.3543941).
- [25] Wentao Wu, Zhirong Lin, Zhi Ni, Peizhan Li, Tiantian Liang, Guofeng Zhang, Yongliang Wang, Liliang Ying, Wei Peng, Wen Zhang, et al. Development of series squid array with on-chip filter for tes detector. *Chinese Physics B*, 31(2):028504, 2022. DOI: [10.1088/1674-1056/ac2b91](https://doi.org/10.1088/1674-1056/ac2b91).

- [26] Barry Muhlfelder, Warren Johnson, and M Cromar. Double transformer coupling to a very low noise squid. *IEEE Transactions on Magnetics*, 19(3):303–307, 2003. DOI: [10.1109/TMAG.1983.1062527](https://doi.org/10.1109/TMAG.1983.1062527).
- [27] V Polushkin, E Gu, D Glowacka, D Goldie, and J Lumley. A tightly coupled dc squid with an intermediary transformer. *Physica C: Superconductivity*, 367(1-4):280–284, 2002. DOI: [10.1016/S0921-4534\(01\)01052-8](https://doi.org/10.1016/S0921-4534(01)01052-8).
- [28] Dietmar Drung, C Abmann, J Beyer, A Kirste, M Peters, F Rueude, and Th Schurig. Highly sensitive and easy-to-use squid sensors. *IEEE Transactions on Applied Superconductivity*, 17(2):699–704, 2007. DOI: [10.1109/TASC.2007.897403](https://doi.org/10.1109/TASC.2007.897403).
- [29] P Falferi, R Mezzena, M Mück, and A Vinante. Cooling fins to limit the hot-electron effect in dc squids. In *Journal of Physics: Conference Series*, volume 97, page 012092. IOP Publishing, 2008. DOI: [10.1088/1742-6596/97/1/012092](https://doi.org/10.1088/1742-6596/97/1/012092).
- [30] Gen Uehara, Naoki Matsuda, Kunio Kazami, and Youichi Takada Kado. Asymmetric bias injection technique for drung-type superconducting quantum interference devices. *Japanese journal of applied physics*, 32(12A):L1735, 1993. DOI: [10.1143/JJAP.32.L1735](https://doi.org/10.1143/JJAP.32.L1735).
- [31] Liliang Ying, Xue Zhang, Minghui Niu, Jie Ren, Wei Peng, Masaaki Maezawa, and Zhen Wang. Development of multi-layer fabrication process for sfq large scale integrated digital circuits. *IEEE Transactions on Applied Superconductivity*, 31(5):1–4, 2021. DOI: [10.1109/TASC.2021.3065277](https://doi.org/10.1109/TASC.2021.3065277).
- [32] Dietmar Drung, Colmar Hinnrichs, and Henry-Jobes Barthelmess. Low-noise ultra-high-speed dc squid readout electronics. *Superconductor Science and Technology*, 19(5):S235, 2006. DOI: [10.1088/0953-2048/19/5/S15](https://doi.org/10.1088/0953-2048/19/5/S15).
- [33] A Kawakami, Y Uzawa, and Z Wang. Josephson array oscillators with microstrip resonators. *IEEE transactions on applied superconductivity*, 7(2):3126–3129, 2002. DOI: [10.1109/77.621994](https://doi.org/10.1109/77.621994).